Internal Report ITESRE 188/1997

DESIGN OF Ka AND Q BAND CORRUGATED FEED HORNS FOR CMB OBSERVATIONS

F.VILLA[1], M.BERSANELLI[2], N.MANDOLESI[1]

Istituto di Tecnologie e Studio delle Radiazioni Extraterrestri

CONSIGLIO NAZIONALE DELLE RICERCHE

Internal Report ITESRE 188/1997

DESIGN OF Ka AND Q BAND CORRUGATED FEED HORNS FOR CMB OBSERVATIONS

F.Villa[1], M.Bersanelli[2], N.Mandolesi[1]

[1]*Istituto TESRE, CNR, Bologna, Italy*
[2]*Istituto di Fisica Cosmica, CNR, Milano, Italy*

April 1997

Internal Report ITESRE 188/1997

DESIGN OF Ka AND Q BAND CORRUGATED FEED HORNS FOR CMB OBSERVATIONS

F.Villa[1], M.Bersanelli[2], N.Mandolesi[1]

[1]*Istituto TESRE, CNR, Bologna, Italy*
[2]*Istituto di Fisica Cosmica, CNR, Milano, Italy*

SUMMARY —- This report describes the electrical design of conical corrugated feed horns in the Ka-band (30 GHz) and Q-band (41 GHz) with requirements imposed by high-precision Cosmic Microwave Background experiments. We outline the design strategy and present results of simulations of the expected beam pattern and return-loss properties performed using a dedicated software package.

1 Introduction

Observations of the Cosmic Microwave Background (CMB) anisotropies require high-quality (low-loss, low sidelobe, low reflection) antennas in the microwave to sub-millimeter range. In particular, ESA's forthcoming space mission Planck Surveyor and precursor balloon-borne experiments such as the UCSB/CNR project BEAST will use arrays of corrugated horns to feed HEMT–based low noise radiometers at frequencies in the 30-120 GHz range (Bersanelli et al. 1996, Mandolesi et al. 1995). Conical corrugated horns are known to exhibit the high beam symmetry, hard beam slope, low sidelobes over a wide bandwidth (e.g. Janssen et al. 1979), characteristics required by high sensitivity astrophysical microwave measurements. The desirable propreties of axial-beam symmetry, low side-lobes, low cross-polarization can be obtained over a wide frequency range in a conical horn that supports the hybrid HE_{11} propagation mode. This mode is a mixture of TE_{11} and TM_{11} modes of the form

$$HE_{11} = TM_{11} + \gamma TE_{11} \tag{1}$$

where γ is a parameter called the *mode-content factor*.

Electrical considerations show that the HE_{11} mode propagates into a waveguide under the following conditions: a) axial reactance X_z and azimuthal reactance X_Φ are different; b) $X_\Phi \to 0$ while $X_z \to \infty$. If these conditions are satisfied, then the TE and TM components are locked together and they propagate with a unique, common velocity. Typically, the hybrid mode propagation condition is obtained by cutting circumferential slots into the inner surfrace of the horn. This configuration is called *Conical Corrugated Horn* and it is widely employed in radio astronomy experiments.

In this report we describe the design and realization of two conical corrugated horns in the 25-35GHz and 38-45GHz bands, to be employed in the BEAST test balloon flight (UCSB/CNR) and which serve as prototypes in view of the Low Frequency Instrument of Planck.

2 Requirements and design strategy

The specific requirements on our prototypes are here summarized:

- flare angle of 7°
- HPBW = 20°
- first side-lobe level < -30 dB respect to maximum
- cross-polarization < 10 dB at $\phi = 45°$

A preliminary prediction of the radiation field was obtained using the spherical wave expansion method (SWEX) under balanced-hybrid condition (i.e. $\gamma = 1$). The transverse electric and magnetic vector fields at the horn aperture are expanded using associate Legendre functions. The radiation pattern can be obtained by integration over the spherical wave surface. SWEX permits to obtain preliminary horn configuration parameters, such as aperture diameter, flare angle, and an approximate level of the first side-lobe.

To reach a more accurate definition of the horn configuration (e.g. slot depth, flared section of the horn) a cascade analysis of slot structure has been performed. Each slot is represented in term of an admittance matrix. The cascade analysis is computed from horn aperture down to the flared region of the horn. This analysis permits an accurate evaluation of the return-loss and the far-field pattern radiation up to the first side-lobe. The (FORTRAN) software accepts an input file containing model structures (slot, ridge, flares, and so on) defined in a cylindrical simmetry, and informaton on the band limits and step frequency. The code analyzes the discontinuity at the aperture (flanged aperture, thin wall aperture, corrugated aperture). Cuts in Θ and Φ can be defined for the pattern radiation. Output data are: electrical field in Θ and Φ cut defined; Radiation pattern in dBi; S11 (return-loss) scattering coefficient.

3 Electrical design

Corrugated horns are composed by four main parts (see Figure 1):

1. The aperture diameter and flare angle which principally determine the beamwidth.
2. The corrugations, which determine pattern simmetry and cross-polar characteristics.
3. Flare section between the throat and the aperture (transition region) which determines the position of the phase center and the hybrid mode propagation along the horn.
4. The throat region, which determines the impedance match between the horn and the waveguide.

Although extensive studies of corrugated horn antennas have been performed (e.g. Blake 1966, Clarricoats & Olver 1984, Johnson & Jasik 1984, Johnson 1991, Uher, Bornemann & Rosenberg 1993) there is no standard procedure for optimized designs. The following procedure has been adopted for our purposes.

3.1 Preliminary definition

The first step leads to a preliminary design based on the choice of the aperture diameter and diameter of the waveguide at the throat region. The aperture diameter has been calculated according to the required HPBW (20°) using the above mentioned SWEX method.

Concerning the waveguide diameter, a circular waveguide is seen as a high-pass filter with a cut-off frequency

$$\nu_c = \frac{c}{\lambda_c} \tag{2}$$

where

$$\lambda_c = D_{m,n} \cdot \frac{D_w}{2} \tag{3}$$

λ_c is the cut-off wavelength, c is the velocity of light in vacuum, and $D_{m,n}$ is a coefficient which depends on the propagated mode. In this case the propagated mode in a circular waveguide is only the $TE_{1,1}$ (equivalent at $TE_{1,0}$ mode in a rectangular waveguide), which gives $D_{1,1} = 3.412$. D_w is the diameter of circular waveguide.

Taking into accout the frequency band we estimate that, for the two horns, the diameter of circular waveguide must be:

$$D_w^{(20-30)} > 10 \text{ mm} \tag{4}$$

$$D_w^{(38-45)} > 5 \text{ mm} \tag{5}$$

3.2 Corrugation geometry

The next step is the choice of corrugation geometry. The main limit is the technical realization. Because a direct machining on a lathe is assumed, the width of corrugations must be sufficiently large. In other world the number of corrugations (fixed the flare angle and the diameter of aperture - *i.e.* the lenght of the horn -) can't be very high. Approximate calculation shows that:

<u>25-35GHz Horn</u>

- Aperture Diameter: $A \simeq 40$ mm
- Waveguide Diameter: $D_w \simeq 10$ mm
- Flare angle: $\Theta_F = 7°$
- Flare Lenght: $L_F = \frac{(A-D_w)}{2 \cdot \sin \Theta_F} \simeq 120$ mm
- Corrugation Width: $b \sim 3$ mm (slot width + ridge width) [1]
- Number of corrugations: $N_c \simeq 40$

[1] *Experimental results show that a good choice of slot width to ridge width ratio is* 0.5

38-45GHz Horn

- Diameter: $A \simeq 25$ mm
- Waveguide Diameter $D_w \sim 5$ mm
- Flare angle: $\Theta_F = 7°$
- Flare Lenght: $L_F = \frac{(A-D_w)}{2 \cdot \sin \Theta_F} \simeq 80$
- Corrugation Width: $b \sim$ 2 mm (slot width + ridge width)
- Number of corrugations: $N_c \simeq 40$

3.3 Detailed analysis

The parameters given in the previous sections are used as input values for a more refined software analysis. A complete program package (described in Section 2) yields an optimization of these parameters in order to obtain the final project.

Final results and project designs are reported in the tables below (Legend of tables is shows in figure 2) and in figures 4 and 5. We have reported also the corrugation profile as a function of corrugation position along horn-axis (Figures 3). These figures show that the inner corrugations are adjusted indipendently in order to obtain a good return-loss. The shape of corrugations in the transition region is essentially linear.

For each horn we show the mechanical drawings (Figures 4 and 5) and the tables containing detailed informations on the the corrugations (table 1 and table 2).

25-35GHz Horn

- Aperture Diameter: $A = 37.71$ mm
- Waveguide Diameter: $D_w = 12.66$ mm
- Flare angle: $\Theta_F = 7°$
- Flare Lenght: $L_F = 102.77$ mm
- Slot Width: $w_s = 2$ mm
- Ridge Width: $w_r = 1$ mm
- Number of corrugations: $N_c = 34$

38-45GHz Horn

- Diameter: $A = 27.16$ mm
- Waveguide Diameter $D_w = 9.04$ mm
- Flare angle: $\Theta_F = 7°$
- Flare Lenght: $L_F = 74.34$
- Slot Width: $w_s = 1.45$ mm
- Ridge Width: $w_r = 0.72$ mm
- Number of corrugations: $N_c = 34$

4 Patterns and Return Loss

Simulations of radiation patterns for each horn are shown in Figures 6,7,8, and 9, using a Cartesian coordinate system (see figure 1). We report the beam patterns in the principal planes (E-plane - $\Phi = 0^0$ and, H-plane - $\Phi = 90^0$) at frequency band extremes: 25GHz and 35GHz for the low frequencies of the horns, 38GHz and 45GHz for the high frequencies. At the middle frequencies: 30GHz and 41.5GHz. For the 25-35GHz horn, radiation patten at 28GHz is also reported (Figure 8). Simulations of return-loss as a function of frequency are displayed in Figure 10. For these simulations, a -30 dB upper limit on return-loss was assumed.

The fabrication process of the horns, as well as of circular-rectangular transitions, is being finalized at IFCTR-CNR Milano. Forthcoming technical reports will describe the construction and performance testing of these components.

ACKNOWLEDGEMENTS

It is a pleasure to thank E.Pagana for his support and countless useful discussions.

REFERENCES

Bersanelli, M., Bouchet, F.R., Efstathiou, G., Griffin, M., Lamarre, J.M., Mandolesi, N., Norgaard–Nielsen, H.U., Polny, J., Vittorio, N., Pace, O., Tauber, J., Volonte', S. 1996, COBRAS/SAMBA Report on the Phase A Study, ESA D/SCI(96)3.

L.V.Blake, *Antennas*, Jhon Wiley & Sons, 1966

P.J.B.Clarricoats, and A.D.Olver *Corrugated Horns for Microwave Antennas*, IEE Electromagnetic Waves Series 18, 1984

R.C.Johnson, H.Jasik, *Antenna Engineering Handbook*,McGraw-Hill Book Conpany,1984

R.C.Johnson, *Designer Notes for Microwave Antennas*, Artech House, 1991

Janssen, M., Bednarczyk, S.M., Gulkis, S., Marlin, H.W., and Smoot, G.F. 1979, IEEE Trans. Antenna Propagat., 27, 551.

Mandolesi, N., et al. 1995, Astroph. Lett & Comm., 32, 309.

J.Uher, J. Bornemann, U. Rosenberg, *Waveguide Components for Antenna Feed Systems: Theory and CAD*, Artech House, 1993

FIGURE CAPTIONS

- FIGURE 1 – Relevant regions of corrugated horn design are reported in the top of this figure. In the bottom, the coordinate system that define the planes of polarization are displayed. E-plane for $\Phi = 0^o$ and H-plane for $\Phi = 90^o$ (from P.J.B. Clarricoats, 1984).

- FIGURE 2 – Definition parameters of a corrugation along the horn profile: W_r is the ridge width, slot width W_s is the slot width, D_r is the ridge diameter, D_s is the slot diameter, and X_s is the slot position along horn axis, starting at the horn aperture. For details see table 1 and table 2.

- FIGURE 3 – Corrugation depth (in mm) as a function of distance from the aperture plane. The inner corrugations ($n_c > 30$) are adjusted indipendently in order to obtain a good return-loss. Corrugations near the aperture plane ($n_c < 13$) have the same depth. The corrugations of transition region have the depth that increase linearly with the distance of the aperture plane.

- FIGURE 4 – Schematic design of conical corrugated horn at 25-35 GHz.

- FIGURE 5 – Schematic design of conical corrugated horn at 38-41 Ghz.

- FIGURE 6 – Ka Band horn: Directivity as a function of ange for E-plane (solid line) and H-plane (dashed line) radiation pattern at 25 GHz and 28 GHz.

- FIGURE 7 – Ka band horn: Directivity as a function of angle for E-plane (solid line) and H-plane (dashed line) radiation pattern at 30 GHz and 35 GHz.

- FIGURE 8 – Q band horn: Directivity as a function of angle for E-plane (solid line) and H-plane (dashed line) radiation pattern at 38 GHz and 41.5 GHz.

- FIGURE 9 – Q band horn: Directivity as a function of angle for E-plane (solid line) and H-plane (dashed line) radiation pattern at 45.0 GHz.

- FIGURE 10 – For each corrugated horn, return-loss as a function of frequency is reported. The top figure is the simulation of the Ka-band horn. The bottom figure is the simulation of the Q-band horn.

- FIGURE 1 -

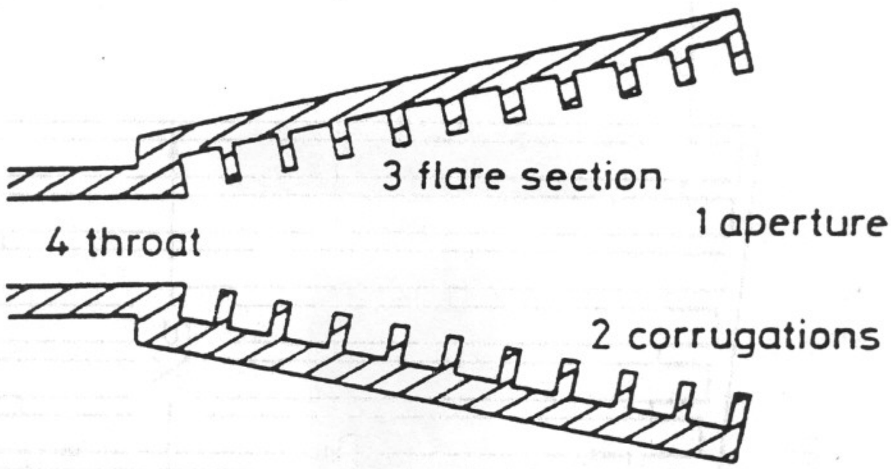

3 flare section
1 aperture
4 throat
2 corrugations

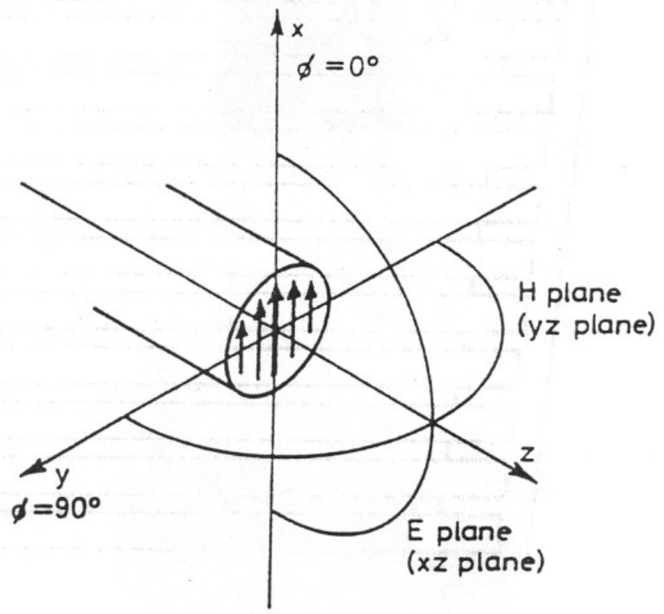

x
$\phi = 0°$
H plane
(yz plane)
z
y
$\phi = 90°$
E plane
(xz plane)

- FIGURE 2 -

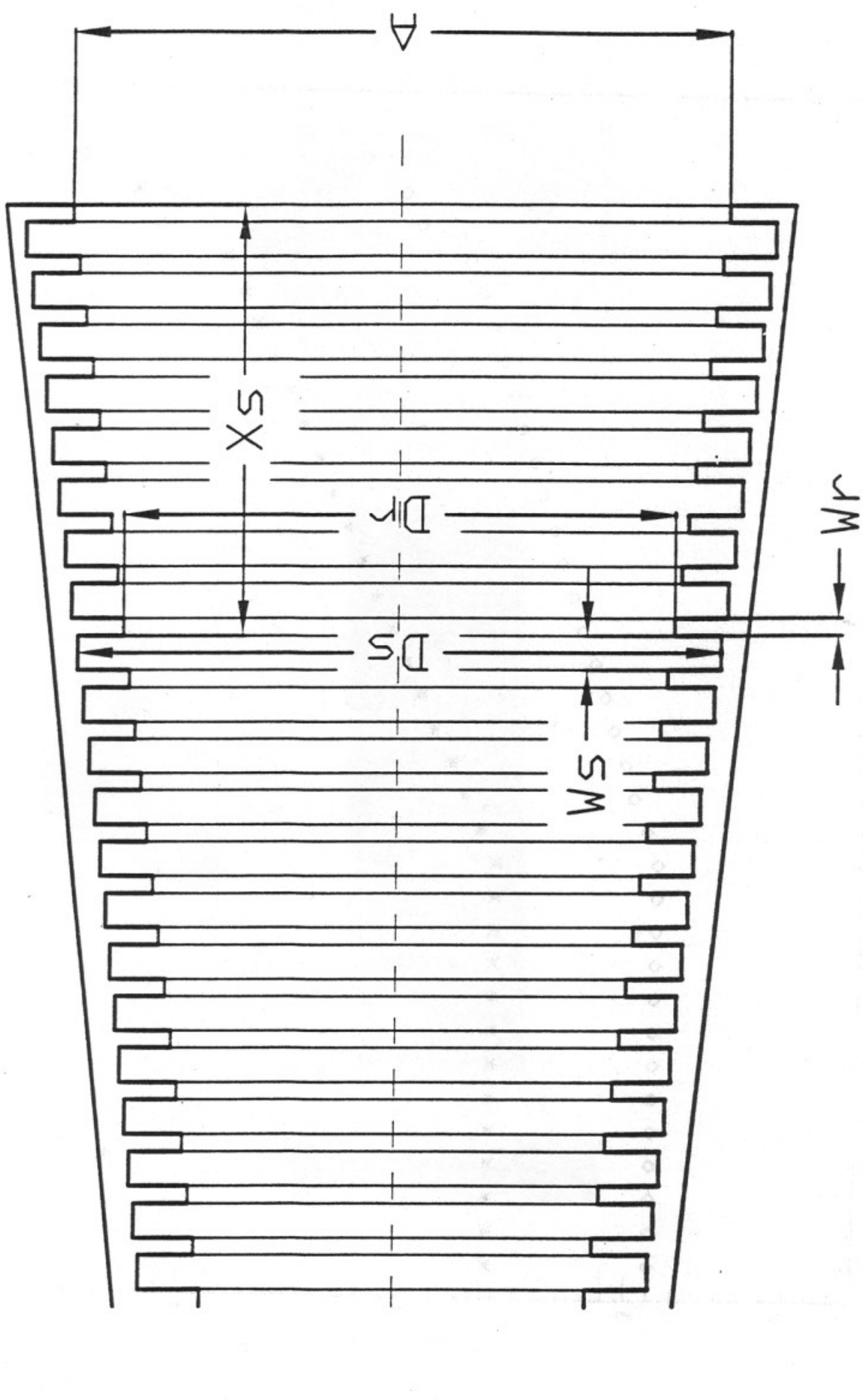

- FIGURE 3 -

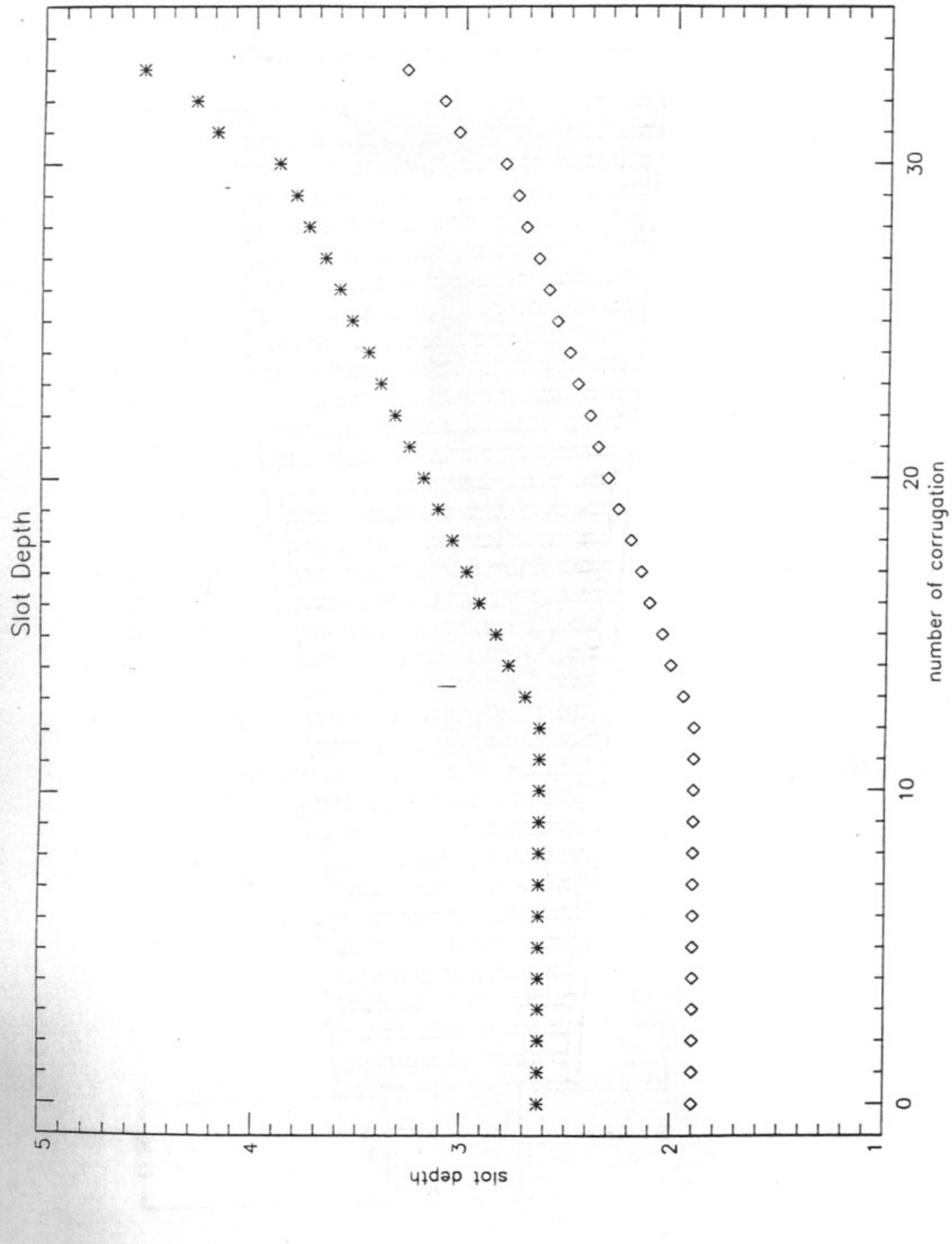

- FIGURE 4 -

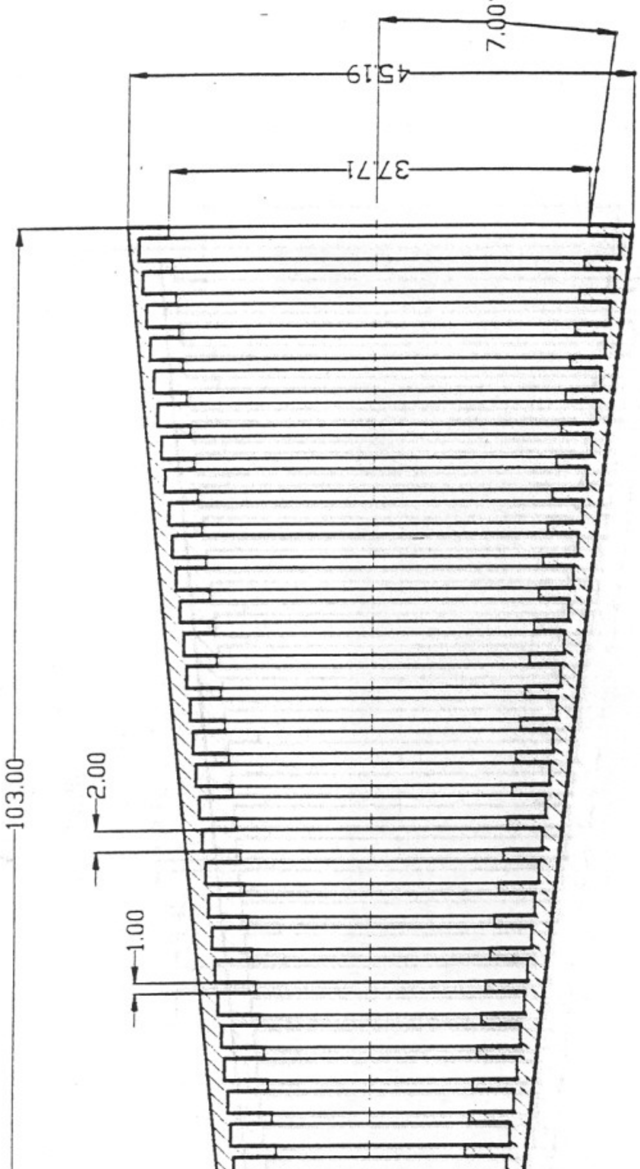

- FIGURE 5 -

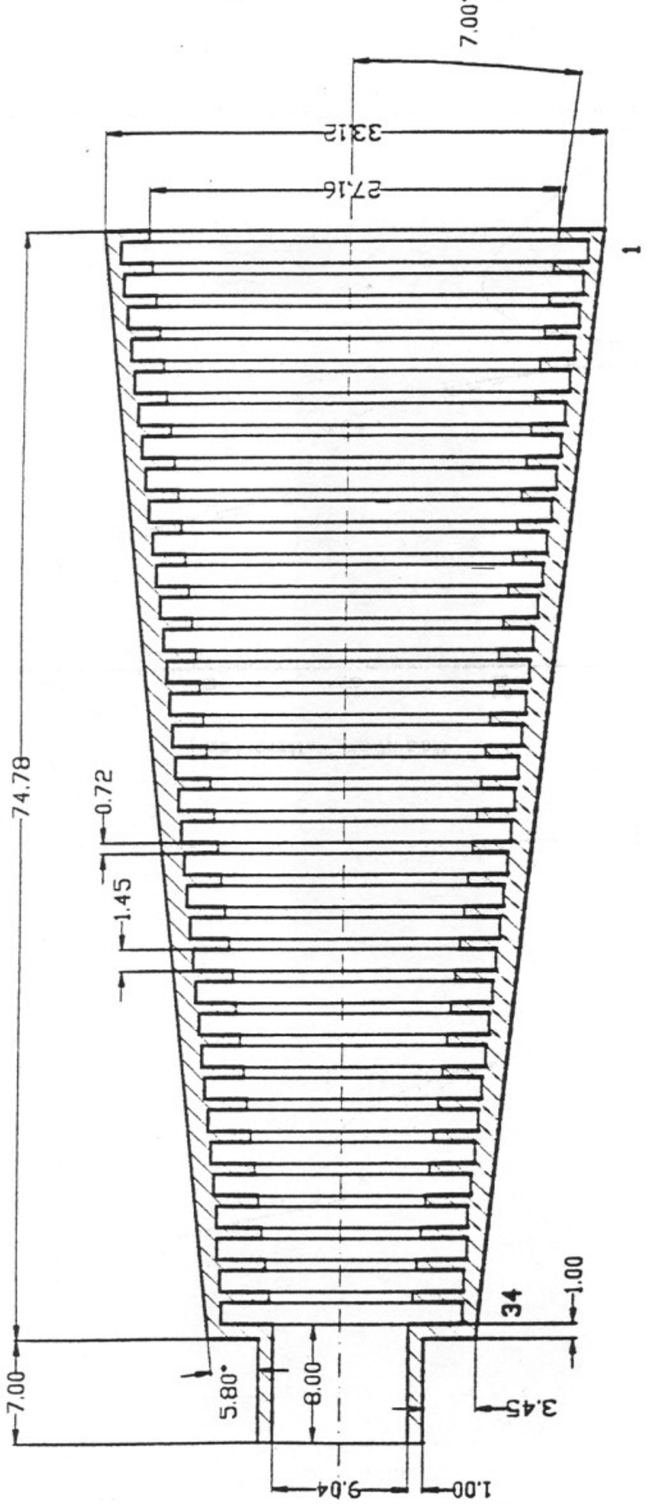

- FIGURE 6 -

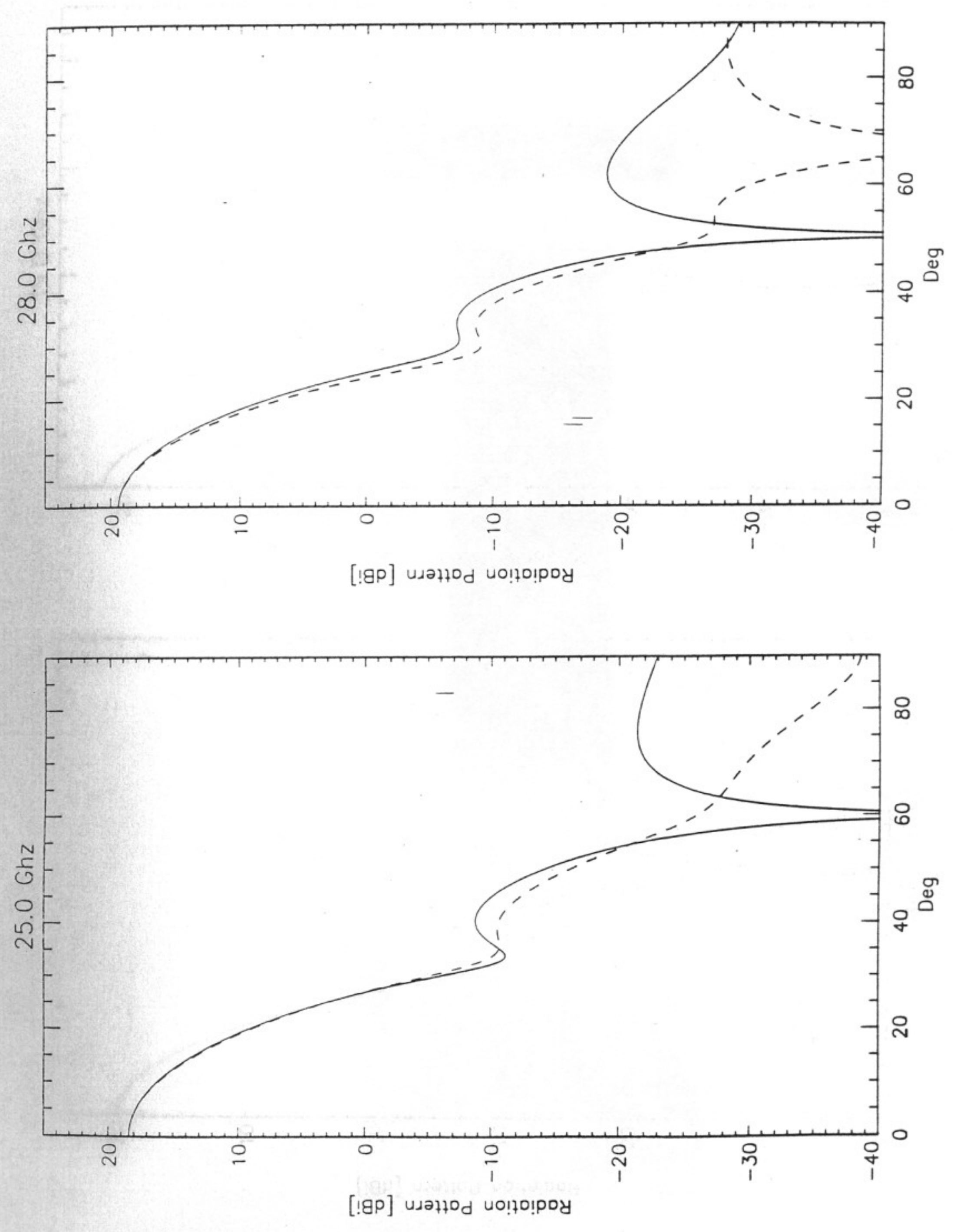
28.0 Ghz
25.0 Ghz
Radiation Pattern [dBi]
Deg
20
10
0
−10
−20
−30
−40
0
20
40
60
80

- FIGURE 7 -

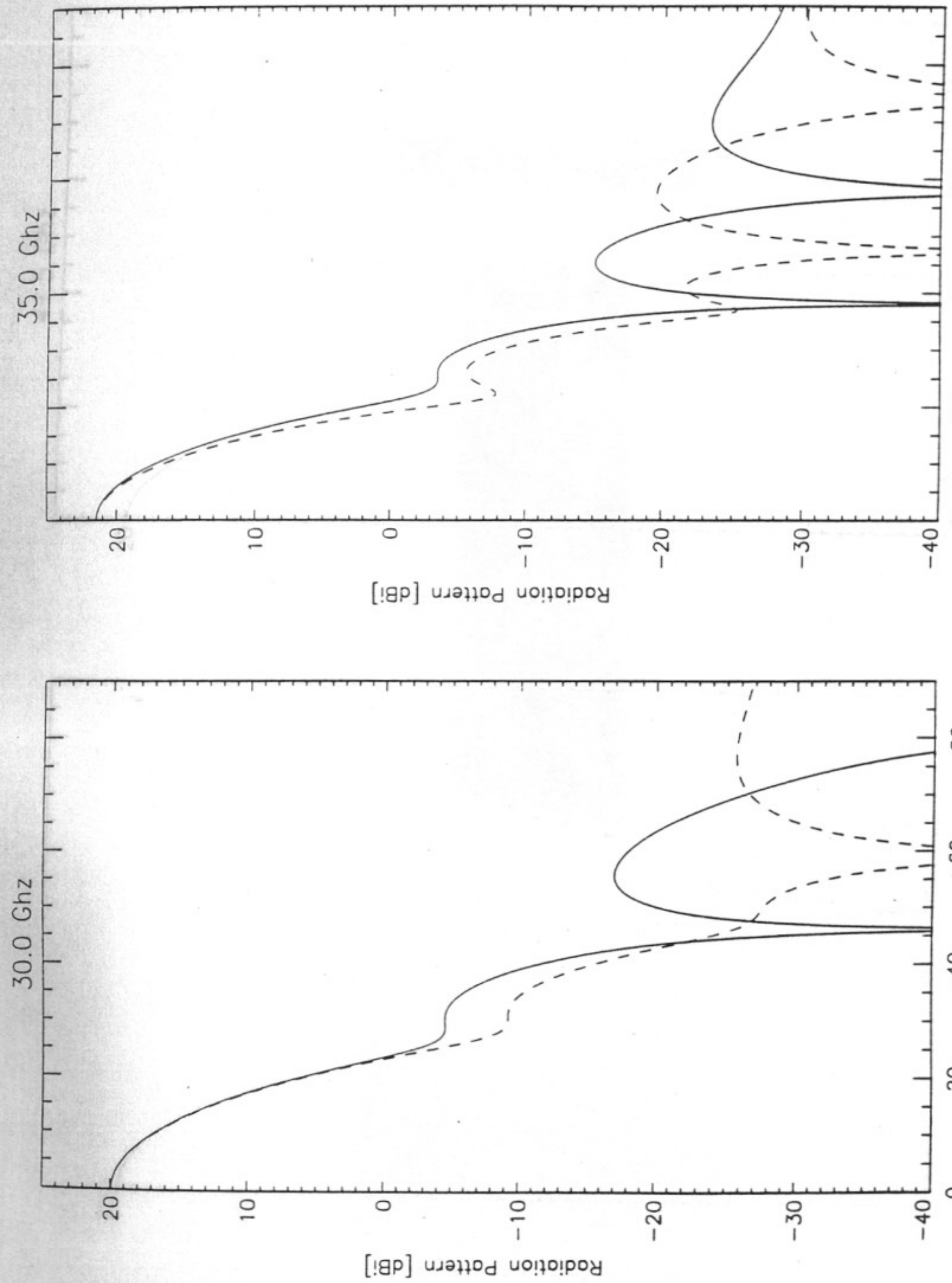

30.0 Ghz
35.0 Ghz
Radiation Pattern [dBi]
Deg
20
10
0
-10
-20
-30
-40
0
20
40
60
80

- FIGURE 8 -

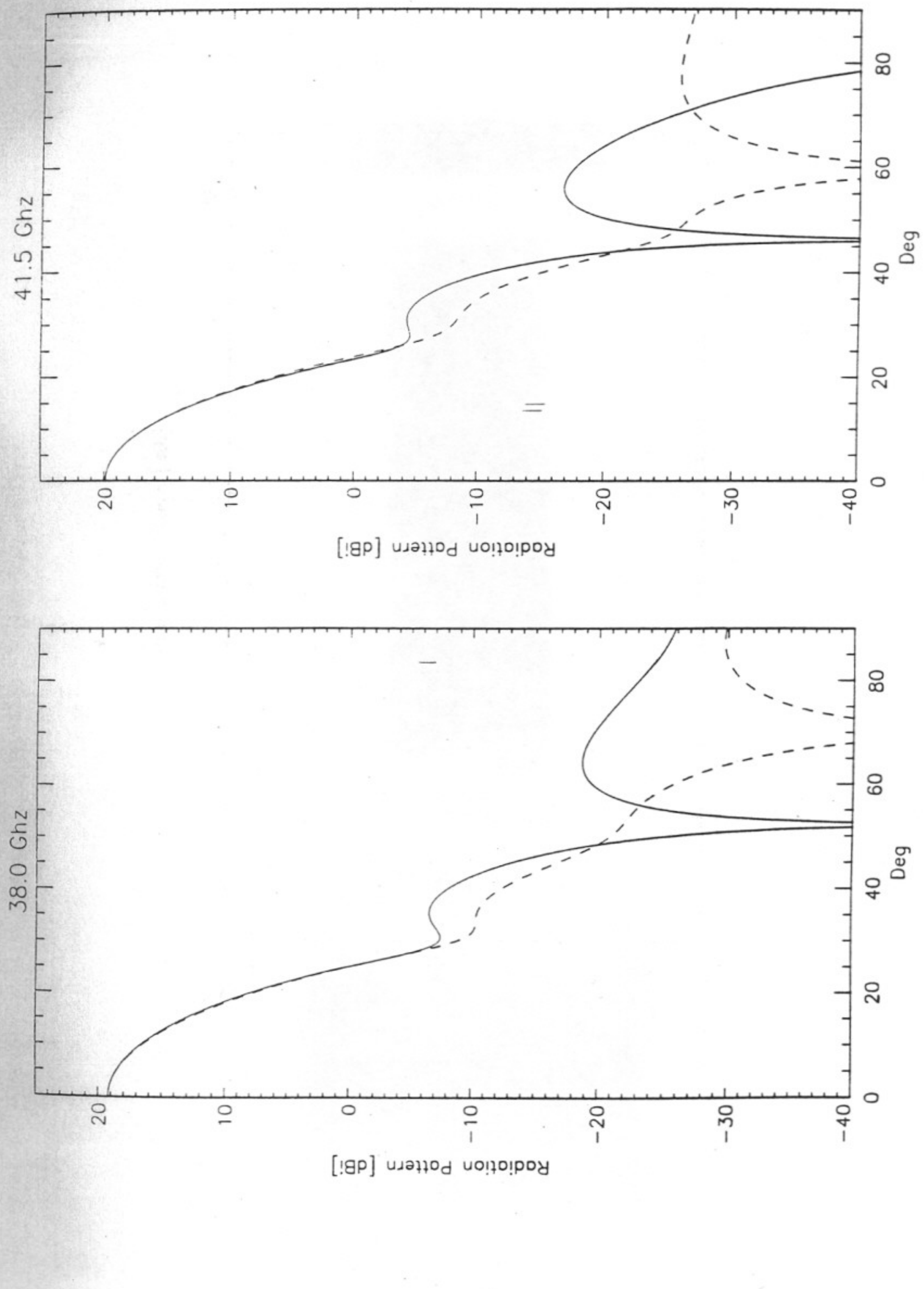

- FIGURE 9 -

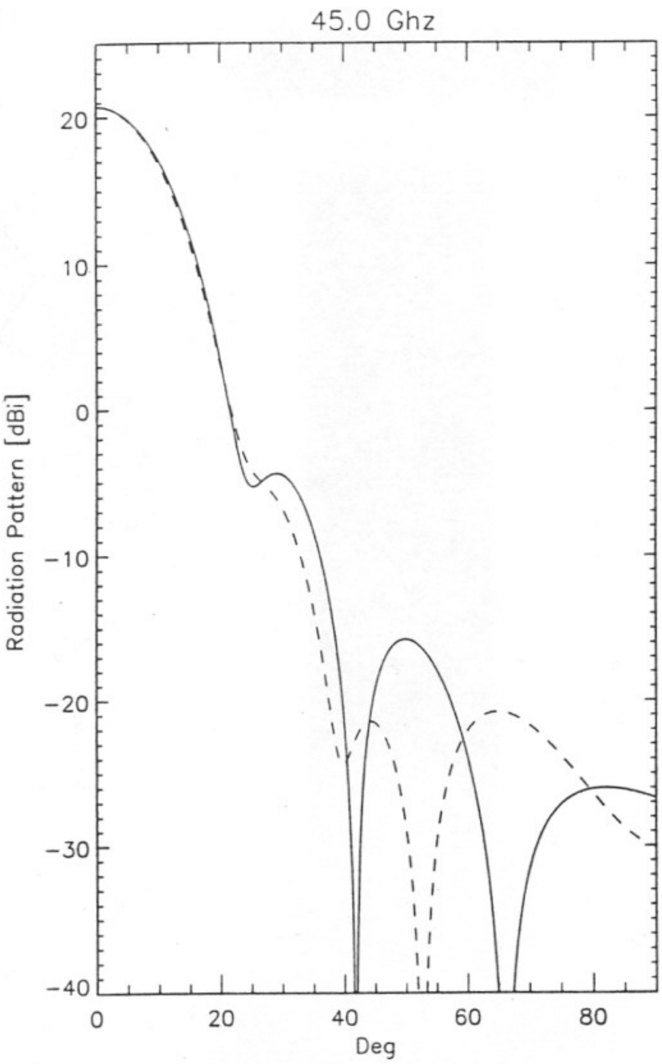
45.0 Ghz
Radiation Pattern [dBi]
Deg
20
10
0
-10
-20
-30
-40
0
20
40
60
80

- FIGURE 10 -

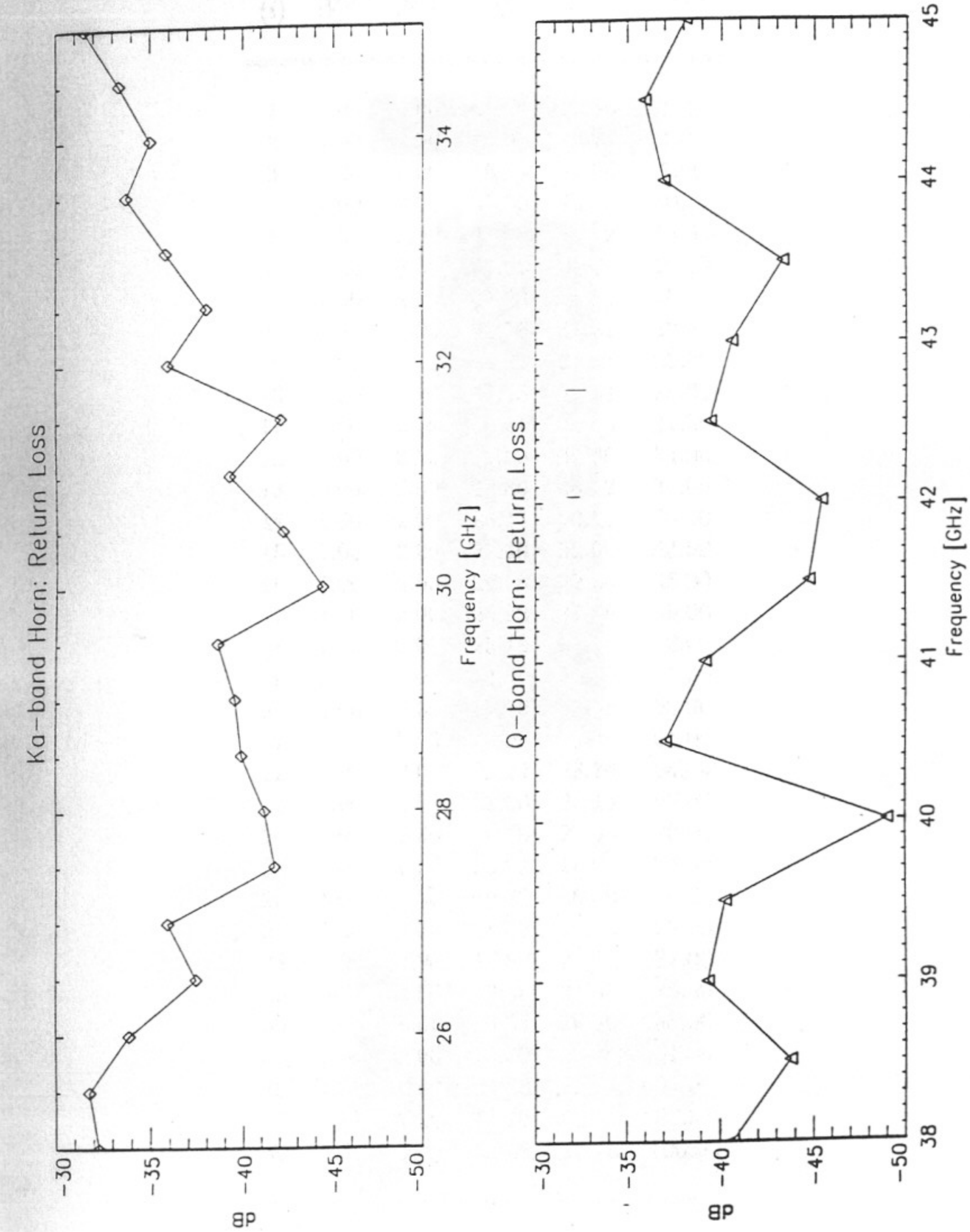

Ka-band Horn: Return Loss
dB
-30
-35
-40
-45
-50
26
28
30
32
34
Frequency [GHz]
Q-band Horn: Return Loss
dB
-30
-35
-40
-45
-50
38
39
40
41
42
43
44
45
Frequency [GHz]

Table 1: horn @ 25-35GHz: corrugation details. for each corrugation (i), ridge width $W_r^{(i)}$, slot width $W_s^{(i)}$, ridge diameter $D_r^{(i)}$, slot diameter $D_s^{(i)}$, and slot position along horn axis, starting from horn aperture $X_s^{(i)}$, are reported in mm.

(i)	$W_r^{(i)}$	$W_s^{(i)}$	$D_r^{(i)}$	$D_s^{(i)}$	$X_s^{(i)}$
1	1.00	2.00	37.70	42.96	1.00
2	1.00	2.00	36.98	42.24	4.00
3	1.00	2.00	36.24	41.50	7.00
4	1.00	2.00	35.50	40.76	10.00
5	1.00	2.00	34.76	40.02	13.00
6	1.00	2.00	34.02	39.28	16.00
7	1.00	2.00	33.28	38.54	19.00
8	1.00	2.00	32.56	37.82	22.00
9	1.00	2.00	31.82	37.08	25.00
10	1.00	2.00	31.08	36.34	28.00
11	1.00	2.00	30.34	35.60	31.00
12	1.00	2.00	29.60	34.86	34.00
13	1.00	2.00	28.86	34.12	37.00
14	1.00	2.00	28.14	33.54	40.00
15	1.00	2.00	27.40	32.96	43.00
16	1.00	2.00	26.66	32.34	46.00
17	1.00	2.00	25.92	31.76	49.00
18	1.00	2.00	25.18	31.14	52.00
19	1.00	2.00	24.44	30.54	55.00
20	1.00	2.00	23.72	29.96	58.00
21	1.00	2.00	22.98	29.36	61.00
22	1.00	2.00	22.24	28.76	64.00
23	1.00	2.00	21.50	28.16	67.00
24	1.00	2.00	20.76	27.56	70.00
25	1.00	2.00	20.02	26.94	73.00
26	1.00	2.00	19.30	26.38	76.00
27	1.00	2.00	18.56	25.76	79.00
28	1.00	2.00	17.82	25.16	82.00
29	1.00	2.00	17.08	24.58	85.00
30	1.00	2.00	16.34	23.96	88.00
31	1.00	2.00	15.60	23.38	91.00
32	1.00	2.00	14.88	23.26	94.00
33	1.00	2.00	14.14	22.72	97.00
34	1.00	2.00	13.40	22.48	100.00

Table 2: horn @ 38-45GHz: corrugation details. for each corrugation (i), ridge width $W_r^{(i)}$, slot width $W_s^{(i)}$, ridge diameter $D_r^{(i)}$, slot diameter $D_s^{(i)}$, and slot position along horn axis, starting at the horn aperture $X_s^{(i)}$, are reported in mm.

(i)	$W_r^{(i)}$	$W_s^{(i)}$	$D_r^{(i)}$	$D_s^{(i)}$	$X_s^{(i)}$
1	0.72	1.45	27.16	30.96	0.72
2	0.72	1.45	26.62	30.42	2.89
3	0.72	1.45	26.10	29.90	5.06
4	0.72	1.45	25.56	29.36	7.23
5	0.72	1.45	25.02	28.82	9.40
6	0.72	1.45	24.50	28.30	11.57
7	0.72	1.45	23.96	27.76	13.74
8	0.72	1.45	23.42	27.22	15.91
9	0.72	1.45	22.90	26.70	18.08
10	0.72	1.45	22.36	26.16	20.25
11	0.72	1.45	21.82	25.62	22.42
12	0.72	1.45	21.30	25.10	24.59
13	0.72	1.45	20.76	24.56	26.76
14	0.72	1.45	20.24	24.14	28.93
15	0.72	1.45	19.70	23.72	31.10
16	0.72	1.45	19.16	23.26	33.27
17	0.72	1.45	18.64	22.86	35.44
18	0.72	1.45	18.10	22.40	37.61
19	0.72	1.45	17.56	21.96	39.78
20	0.72	1.45	17.04	21.56	41.95
21	0.72	1.45	16.50	21.12	44.12
22	0.72	1.45	15.96	20.68	46.29
23	0.72	1.45	15.44	20.24	48.46
24	0.72	1.45	14.90	19.82	50.63
25	0.72	1.45	14.36	19.36	52.80
26	0.72	1.45	13.84	18.96	54.97
27	0.72	1.45	13.30	18.50	57.14
28	0.72	1.45	12.78	18.08	59.31
29	0.72	1.45	12.24	17.66	61.48
30	0.72	1.45	11.70	17.20	63.65
31	0.72	1.45	11.18	16.80	65.82
32	0.72	1.45	10.64	16.70	67.99
33	0.72	1.45	10.10	16.30	70.16
34	0.72	1.45	9.58	16.14	72.33

TESRE-CNR - VIA P. GOBETTI, 101 - 40129 BOLOGNA (ITALY) - TEL. (051) 6398688 - FAX (051) 6398724